Spontaniczne rozszczepienie jąder superciężkich jako emisja klastrów

Michał Warda

Uniwersytet Marii Curie-Skłodowskiej
w Lublinie

Warszawa, 7.12.2017

Collaboration:

- J.L. Egido, UAM, Madrid
- L.M. Robledo, UAM, Madrid
- A. Zdeb, UMCS, Lublin

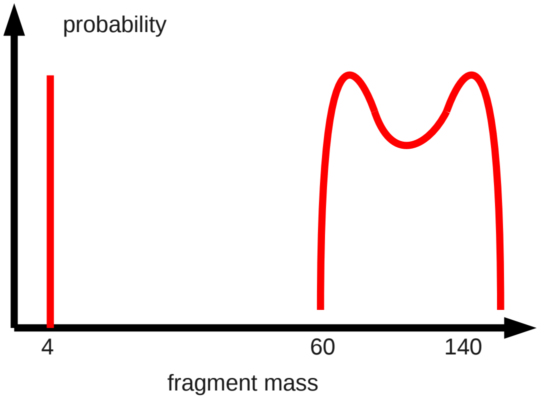
probability
4
60
140
fragment mass

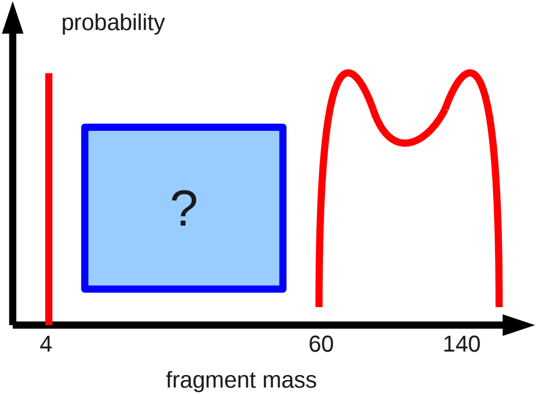
probability
?
4
60
140
fragment mass

Discovery of cluster radioactivity

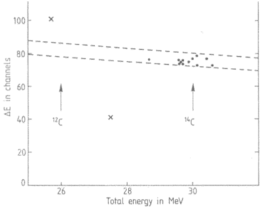

Fig. 1 Contents of the two-dimensional array ΔE versus E_{total} after a run of 189 days. The dotted line indicates the allowed region for carbon ions and the arrows indicate the total energies expected for ^{12}C and ^{14}C emissions in the decay of ^{223}Ra. The lower of the two crosses represents a quadruple pile-up. Below the total energy displayed, large numbers of triple and double α-pile-ups were recorded. Single α-events (and, in part, even double α-pile-ups) were biased out on the analogue side to avoid deadtime problems on the digital side. The upper cross is an event which was recorded during a thunderstorm which affected the mains badly. A run of 194 days was made before this one, yielding 8 events and, in addition, a run of approximately half a year was performed to investigate possible cosmic ray-induced events. Channel 77 in $\Delta E \approx 6.7$ MeV, which is exactly as expected for 30 MeV ^{14}C. Detector characteristics: The dead layer of the ΔE detector (200 mm^2 active area, 8.2 μm sensitive thickness) was determined to lie between 0.3 and 0.8 μm. In addition a protective layer of gold of thickness 20 μg cm^{-2} was evaporated on the source and 15 μg cm^{-2} carbon film inserted between the source and the ΔE detector. An extra 30–40 μg cm^{-2} of gold is present on the E-detector (300 mm^2 active area). This gives a total of 150–250 μg cm^{-2} of effective dead layer (Si equivalent) and an energy loss of ^{14}C ions of 0.5–0.8 MeV. The source of strength 3.3 μCi gave a counting rate of $\approx$4,000 s^{-1}, corresponding to an effective solid angle of detection of $\approx$1/3 sr.

$$^{223}_{88}\mathrm{Ra} \longrightarrow {}^{14}\mathrm{C} + {}^{209}\mathrm{Pb}$$

H.J. Rose and G.A. Jones, *Nature* **307**, 245 (1984)
Sandulescu, Poenaru and Greiner, *Sov. J. Part Nucl.* **11**, 528 (1980)

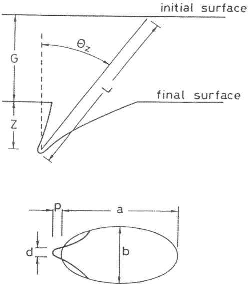

Fig. 1. Geometry of a track etched until the end of the particle range, L. G is the thickness of the material etched away, d the tip diameter, a and b the major and minor axes, p the overhang, Θ_z the zenith angle, z the track depth.

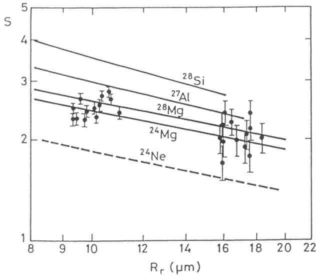

Fig. 6. Comparison of the sensitivity S measured at two stages of the etching process for the 15 events from the decay of ^{236}Pu with accelerator calibrations. Reprinted with permission from M. Hussonnois et al., "Cluster decay of ^{236}Pu and correlations of the probabilities of α decay, cluster decay and spontaneous fission of heavy nuclei" JETP Letters 62 (1995) p 701. Copyright 1995 American Institute of Physics.

R. Bonetti, A. Guglielmetti, in *Heavy Elements and Related New Phenomena Vol II, ed. W. Greiner and R.K. Gupta*, p.634, Word Scientific, 1999

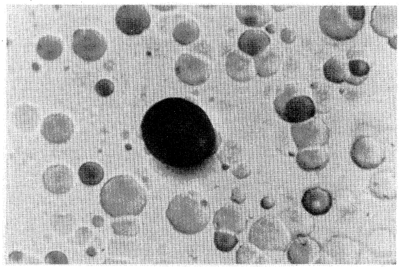

FIG. 1. Photomicrograph showing one etch pit due to a 56 MeV ^{24}Ne ion striking a Cronar detector nearly head on. About 3×10^6 alpha particles passed through this field of view.

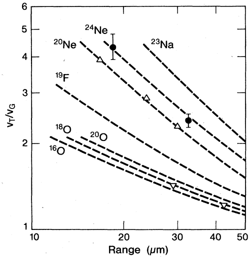

FIG. 2. Comparison of average signal of ^{24}Ne nuclei (●) emitted from ^{232}U with calibrations (dashed lines) obtained with ^{18}O (▽) and ^{20}Ne (Δ) ions at Lawrence Berkeley Laboratory accelerators. Ratio of etching rate along track to general etching rate v_T/v_G, is plotted as a function of residual range.

Barwick et al., PRC **31**, 1984 (1985)

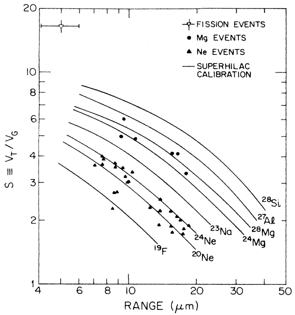

FIG. 1. Identification of ions emitted from ^{234}U as Ne and Mg. The curves are based on calibrations obtained with ^{28}Si, ^{24}Mg, and ^{20}Ne ions at Lawrence Berkeley Laboratory SuperHilac.

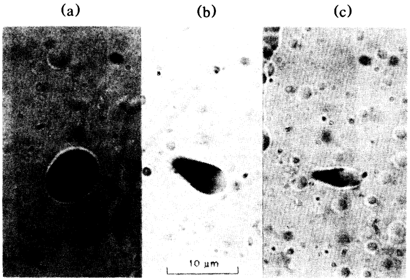

FIG. 2. Photomicrographs showing etch pits due to (a) spontaneous fission, (b) Mg emission, and (c) Ne emission from ^{234}U source.

Wang et al., PRC **36**, 2717 (1987)

Cluster radioactivity: key facts

- Emitters: $^{221}_{87}$Fr — $^{242}_{96}$Cm
  experimental evidence in 12 even-even, 9 odd nuclei
- Clusters: ^{14}C — ^{34}Si
- Heavy mass residue: doubly magic ^{208}Pb ± 4 nucleons
  "Lead radioactivity"
- Half lives: 10^{11} s – 10^{26} s
- α branching ratio: 10^{-9} – 10^{-16}

Cluster radioactivity: key facts

- Emitters: ${}^{221}_{87}$Fr — ${}^{242}_{96}$Cm
  experimental evidence in 12 even-even, 9 odd nuclei
- Clusters: ^{14}C — ^{34}Si
- Heavy mass residue: doubly magic ^{208}Pb ± 4 nucleons
  "Lead radioactivity"
- Half lives: 10^{11} s – 10^{26} s
- α branching ratio: 10^{-9} – 10^{-16}

Cluster radioactivity: key facts

- Emitters: ${}^{221}_{87}$Fr — ${}^{242}_{96}$Cm
  experimental evidence in 12 even-even, 9 odd nuclei
- Clusters: ^{14}C — ^{34}Si
- Heavy mass residue: doubly magic ^{208}Pb ± 4 nucleons
  "Lead radioactivity"
- Half lives: 10^{11} s – 10^{26} s
- α branching ratio: 10^{-9} – 10^{-16}

Cluster radioactivity: key facts

- Emitters: ${}^{221}_{87}$Fr — ${}^{242}_{96}$Cm
  experimental evidence in 12 even-even, 9 odd nuclei
- Clusters: ^{14}C — ^{34}Si
- Heavy mass residue: doubly magic ^{208}Pb ± 4 nucleons
  "Lead radioactivity"
- Half lives: 10^{11} s – 10^{26} s
- α branching ratio: 10^{-9} – 10^{-16}

Cluster radioactivity: key facts

- Emitters: ${}^{221}_{87}$Fr — ${}^{242}_{96}$Cm
  experimental evidence in 12 even-even, 9 odd nuclei
- Clusters: ^{14}C — ^{34}Si
- Heavy mass residue: doubly magic ^{208}Pb ± 4 nucleons
  "Lead radioactivity"
- Half lives: 10^{11} s – 10^{26} s
- α branching ratio: 10^{-9} – 10^{-16}

Cluster radioactivity: key facts

- Emitters: $^{221}_{87}$Fr — $^{242}_{96}$Cm
  experimental evidence in 12 even-even, 9 odd nuclei
- Clusters: ^{14}C — ^{34}Si
- Heavy mass residue: doubly magic ^{208}Pb ± 4 nucleons
  "Lead radioactivity"
- Half lives: 10^{11} s – 10^{26} s
- α branching ratio: 10^{-9} – 10^{-16}

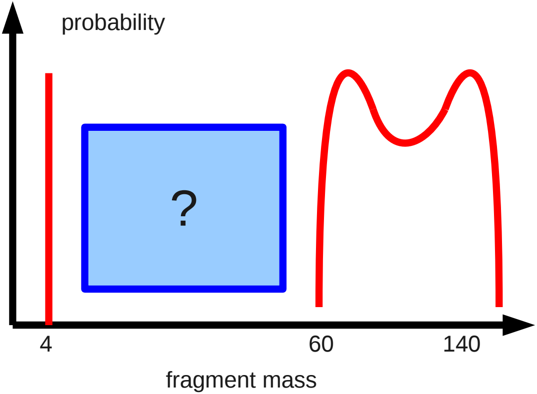
probability
?
4
60
140
fragment mass

Theoretical description

- Extrapolation of Gamov model of alpha emission
  Modified Geiger-Nuttall formula for half-lives

Theoretical description

- Extrapolation of Gamov model of alpha emission
  Modified Geiger-Nuttall formula for half-lives

$$\log_{10} T^{AZ}_{1/2} = \frac{aA_2\eta + bZ_2\eta_z}{\sqrt{Q}} + c.$$

$a = 10.603$, $b = 78.027$, and $c = -80.66$

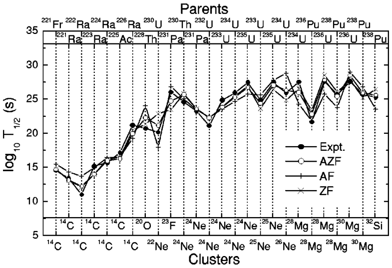

FIG. 1. $\log_{10} T_{1/2}$ (s) for different clusters emitted from various radioactive parents, calculated by using the AZ formula (AZF) and compared with experimental data. Also, the results of calculations for AF ($b = 0$) and ZF ($a = 0$) truncations of AZF are shown for comparisons.

Balasubramaniam et al., PRC **70**, 017301 (2004)

$$\log_{10} T_{1/2} = a\sqrt{\mu} Z_c Z_d Q^{-1/2} + b\sqrt{\mu}(Z_c Z_d)^{1/2} + c$$

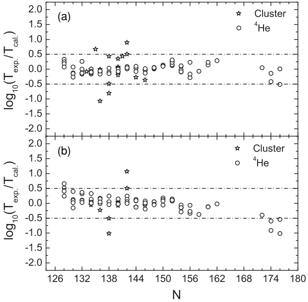

FIG. 4. Deviations between the logarithms of the experimental data and of the calculated values for even-even nuclei (a) when we use two sets of parameters to describe α decay and cluster radioactivity respectively and (b) when we use one set of parameters to describe both α decay and cluster radioactivity at the same time.

Ni et al., PRC **78**, 044310 (2008)

$$V(r) = \begin{cases} -V_0 & 0 \le r \le R \\ \frac{Z_1 Z_2 e^2}{r} & r > R \end{cases}$$

$$R = r_0(A_1^{1/3} + A_2^{1/3})$$

$$b = \frac{Z_1 Z_2 e^2}{E_\mathrm{k}}$$

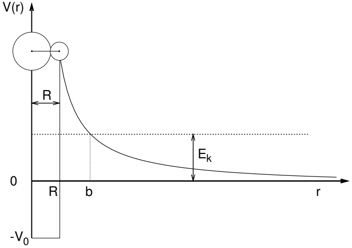

$$P = \exp\left[-\frac{2}{\hbar}\int_R^b \sqrt{2\mu(V(x) - E_k)}dx\right]$$

$$P = \exp\left\{-\frac{2}{\hbar}\sqrt{2\mu Z_1 Z_2 e^2 b}\left[\arccos\sqrt{\frac{R}{b}} - \sqrt{\frac{R}{b} - \left(\frac{R}{b}\right)^2}\right]\right\}$$

A. Zdeb, M. Warda, K. Pomorski, Phys. Rev. C87 024308 (2013)

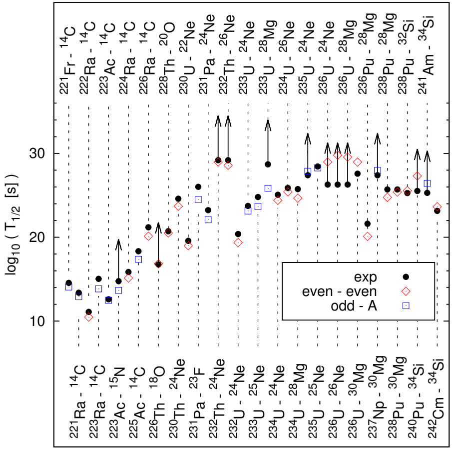

$$T_{1/2} = \frac{\ln 2}{P\nu} \cdot 10^{h}$$
$$\nu = \frac{\pi\hbar}{2\mu R^2}$$

$$r_0 = 1.21 \text{ fm}$$
$$h = 1.973$$

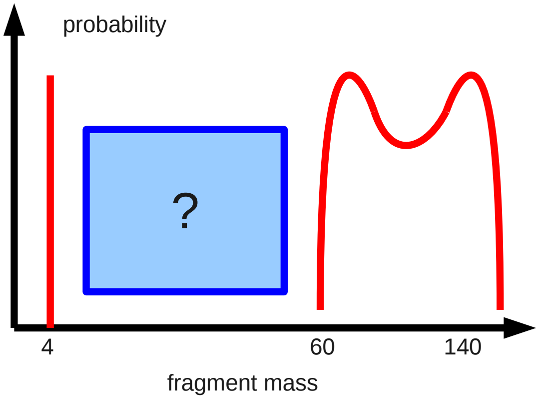
probability
?
4
60
140
fragment mass

Theoretical description

- Very asymmetric fission
- Potential energy surfaces are determined in the self-consistent procedure in HFB theory with Gogny D1S force

Theoretical description

- Very asymmetric fission
- Potential energy surfaces are determined in the self-consistent procedure in HFB theory with Gogny D1S force

www.umcs.lublin.pl

Theoretical description

- Very asymmetric fission
- Potential energy surfaces are determined in the self-consistent procedure in HFB theory with Gogny D1S force

Shape evolution: ^{238}Pu

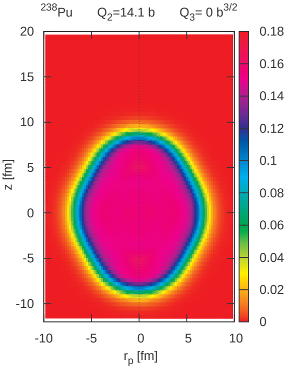

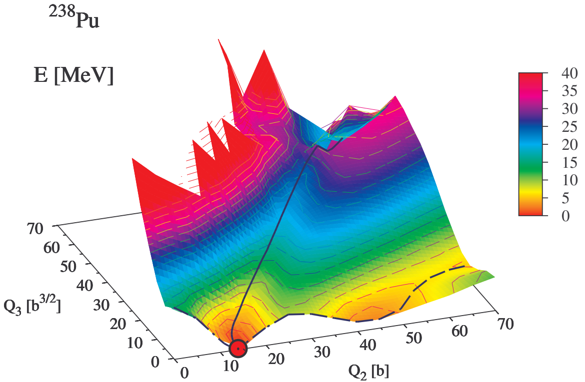

M. Warda and L. M. Robledo, Phys. Rev. C 84, 044608 (2011).

Shape evolution: ^{238}Pu

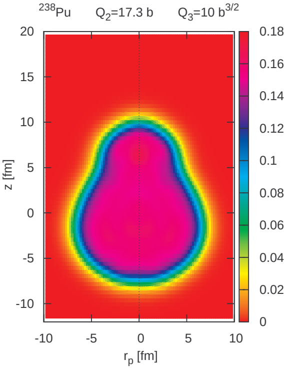

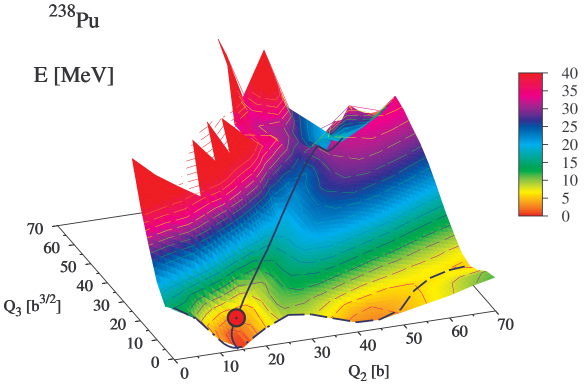

M. Warda and L. M. Robledo, Phys. Rev. C 84, 044608 (2011).

Shape evolution: ^{238}Pu

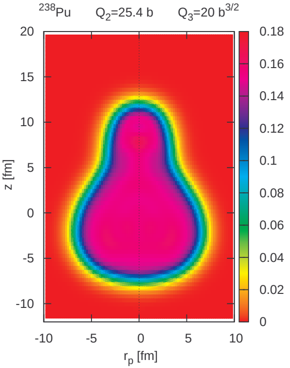

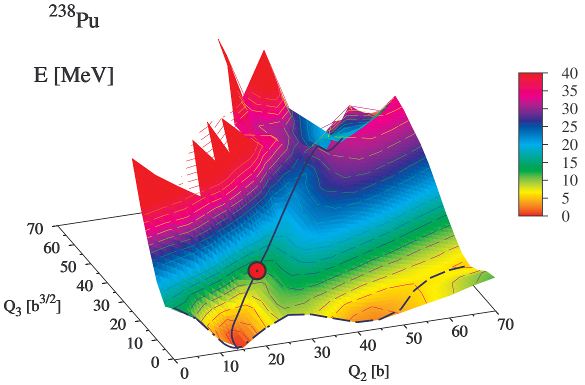

M. Warda and L. M. Robledo, Phys. Rev. C 84, 044608 (2011).

UMCS

Shape evolution: ^{238}Pu

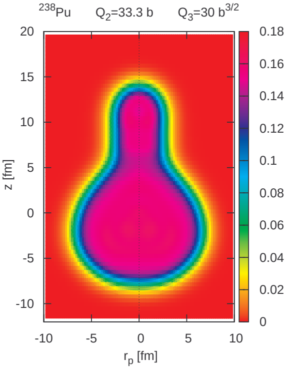

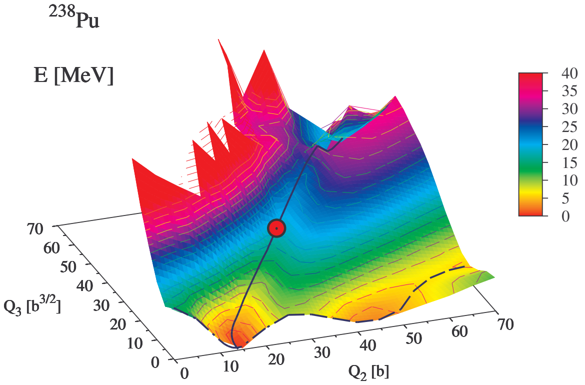

M. Warda and L. M. Robledo, Phys. Rev. C 84, 044608 (2011).

Shape evolution: ^{238}Pu

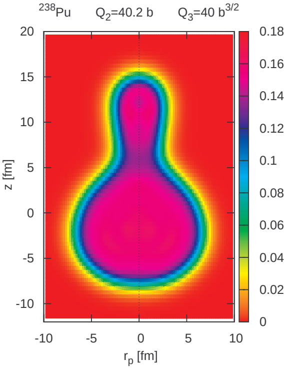

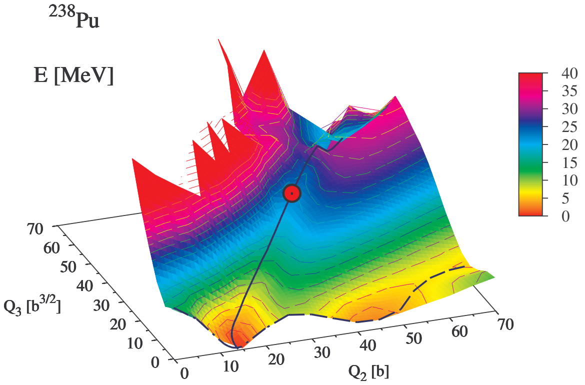

M. Warda and L. M. Robledo, Phys. Rev. C 84, 044608 (2011).

Shape evolution: ^{238}Pu

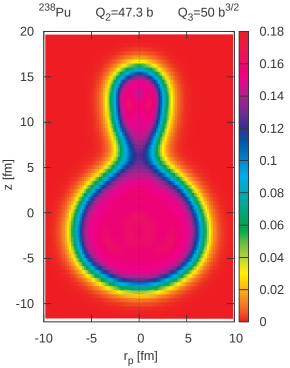

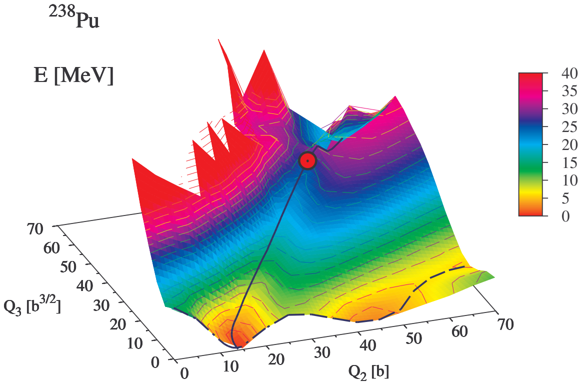

M. Warda and L. M. Robledo, Phys. Rev. C 84, 044608 (2011).

Shape evolution: ^{238}Pu

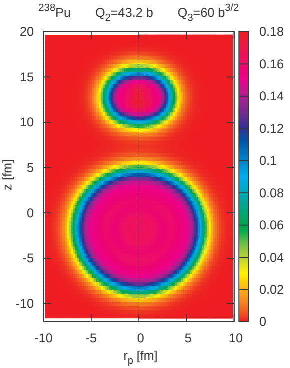

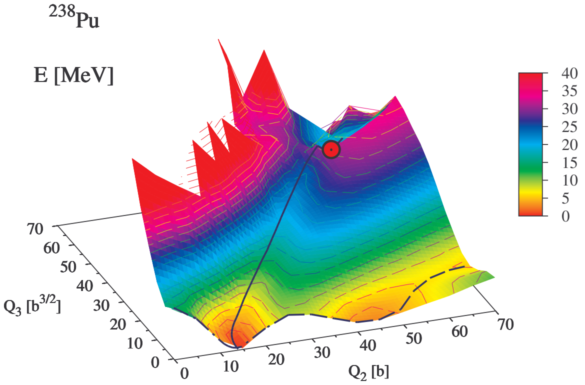

M. Warda and L. M. Robledo, Phys. Rev. C 84, 044608 (2011).

Shape evolution: ^{238}Pu

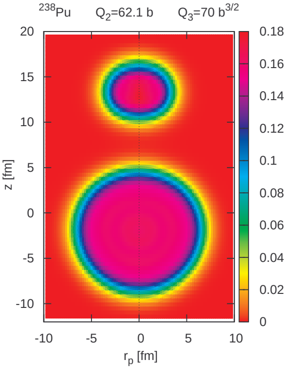

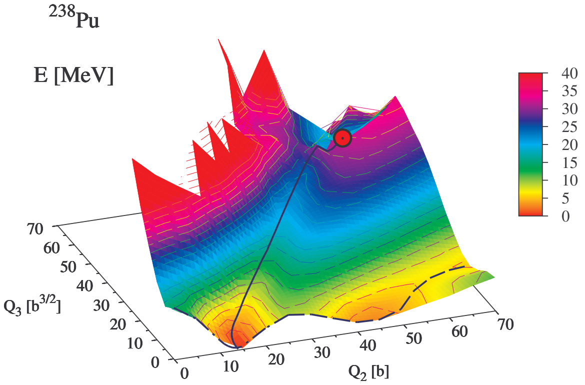

M. Warda and L. M. Robledo, Phys. Rev. C 84, 044608 (2011).

Shape evolution: ^{238}Pu

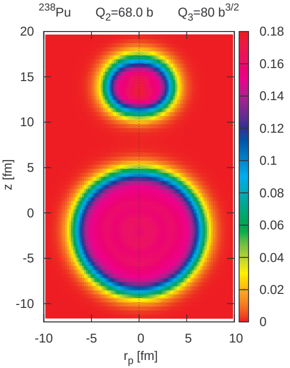

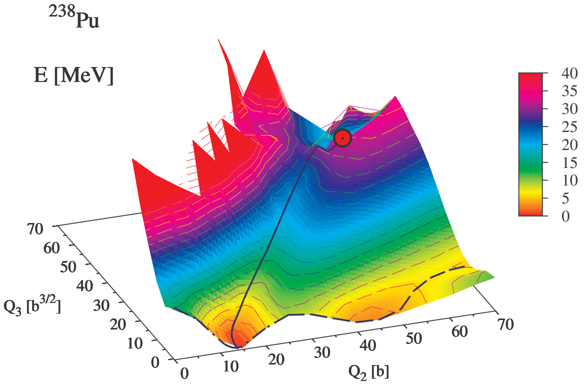

M. Warda and L. M. Robledo, Phys. Rev. C 84, 044608 (2011).

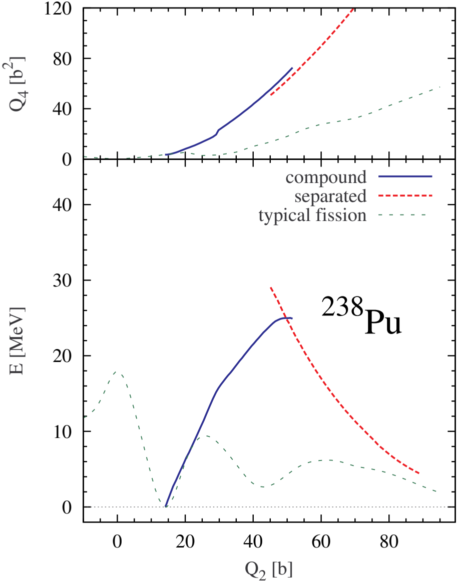
120
80
40
0
Q_4 [b^2]
compound
separated
typical fission
40
30
20
10
0
E [MeV]
^{238}Pu
0
20
40
60
80
Q_2 [b]

Half-lives

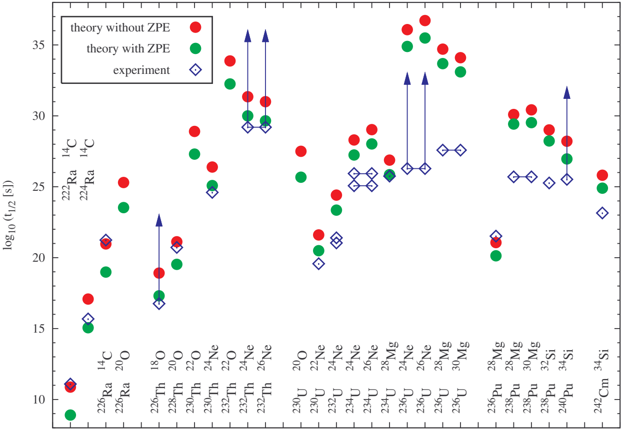
theory without ZPE
theory with ZPE
experiment
$\log_{10}(t_{1/2}\ [s])$
10
15
20
25
30
35
^{222}Ra ^{14}C
^{224}Ra ^{14}C
^{226}Ra ^{14}C
^{226}Ra ^{20}O
^{226}Th ^{18}O
^{228}Th ^{20}O
^{230}Th ^{22}O
^{230}Th ^{24}Ne
^{232}Th ^{22}O
^{232}Th ^{24}Ne
^{232}Th ^{26}Ne
^{230}U ^{20}O
^{230}U ^{22}Ne
^{232}U ^{24}Ne
^{234}U ^{24}Ne
^{234}U ^{26}Ne
^{234}U ^{28}Mg
^{236}U ^{24}Ne
^{236}U ^{26}Ne
^{236}U ^{28}Mg
^{236}U ^{30}Mg
^{236}Pu ^{28}Mg
^{238}Pu ^{28}Mg
^{238}Pu ^{30}Mg
^{238}Pu ^{32}Si
^{240}Pu ^{34}Si
^{242}Cm ^{34}Si

Fission fragments - N/Z ratio

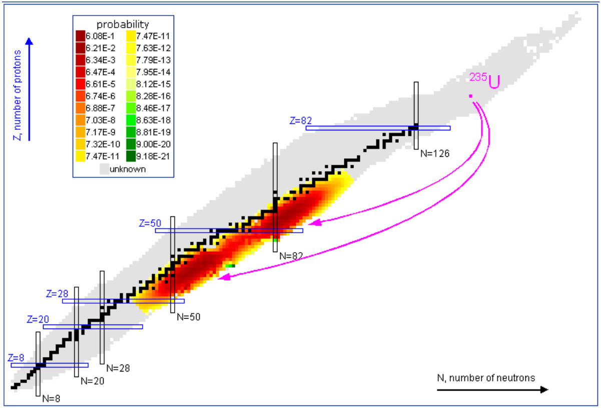

http://lablemminglounge.blogspot.com/2011/03/why-fuel-rods-are-radioactive.html

Fission fragments - N/Z ratio

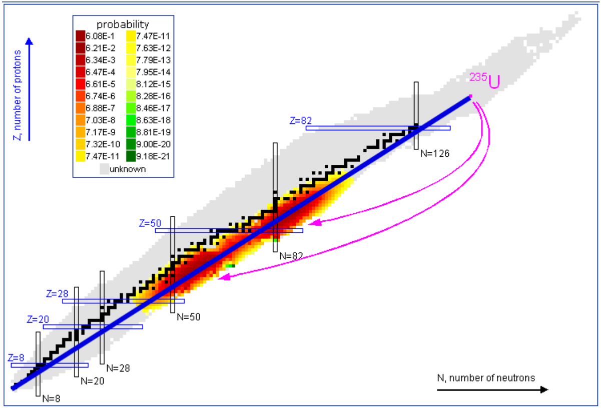

http://lablemminglounge.blogspot.com/2011/03/why-fuel-rods-are-radioactive.html

Cluster radioactivity - chart of nuclides

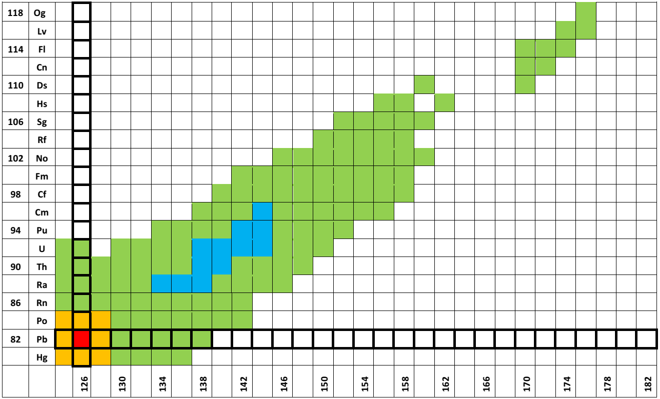

Cluster radioactivity - chart of nuclides

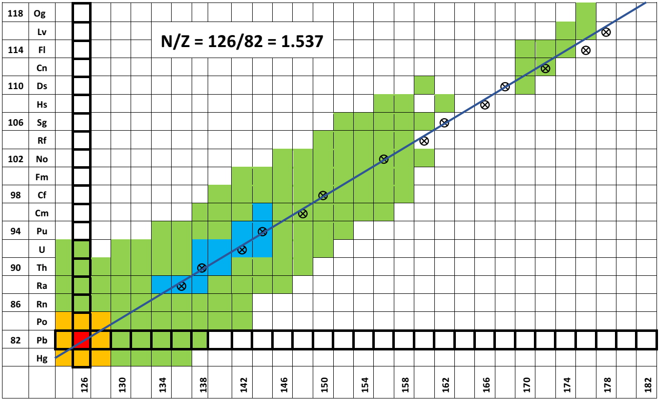

Chart of SH nuclides

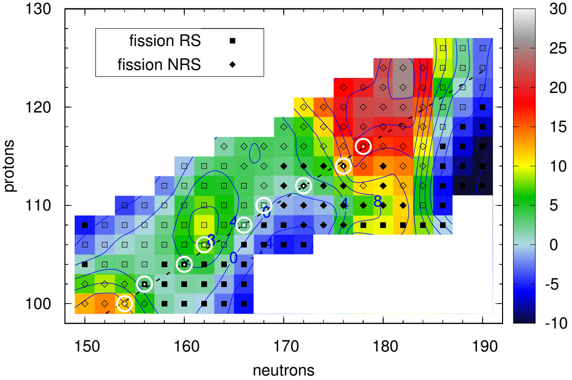

M. Warda, J.L. Egido, Phys. Rev. C 86 (2012) 014322
A. Baran, M. Kowal, P.G. Reinhard, L.M. Robledo, A. Staszczak, M. Warda, Nucl. Phys. A 944 (2015) 442

Fission barriers

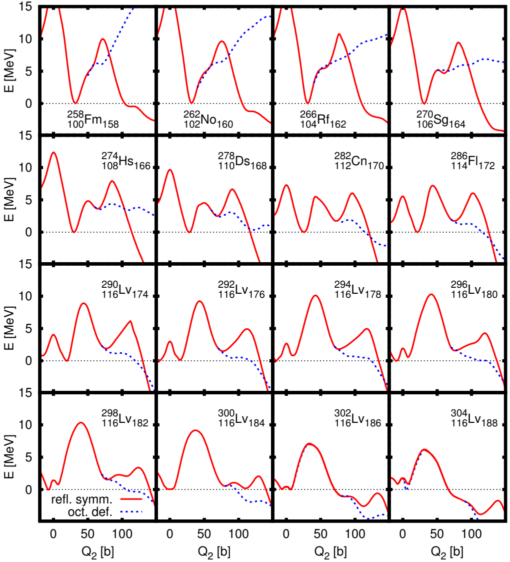

www.umcs.lublin.pl

Fission barriers in ^{274}Hs and ^{282}Cn

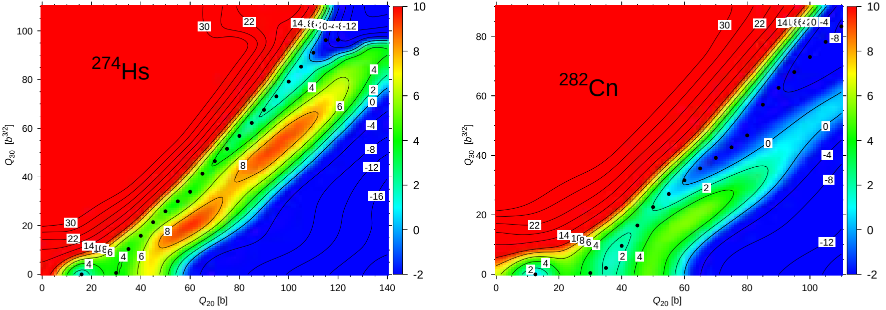

^{266}Hs

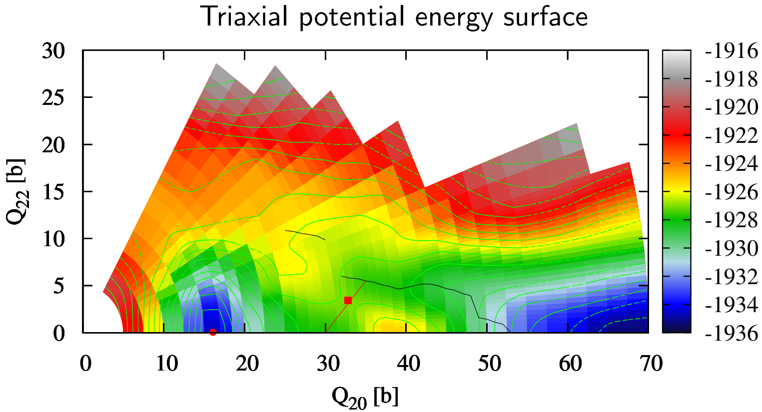
Triaxial potential energy surface
Q22 [b]
Q20 [b]
30
25
20
15
10
5
0
0
10
20
30
40
50
60
70
-1916
-1918
-1920
-1922
-1924
-1926
-1928
-1930
-1932
-1934
-1936

Fission and α-decay half-lives

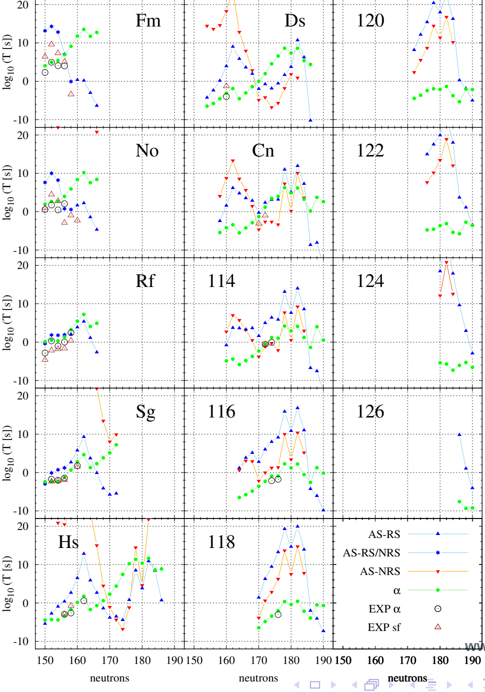

Fission half-lives

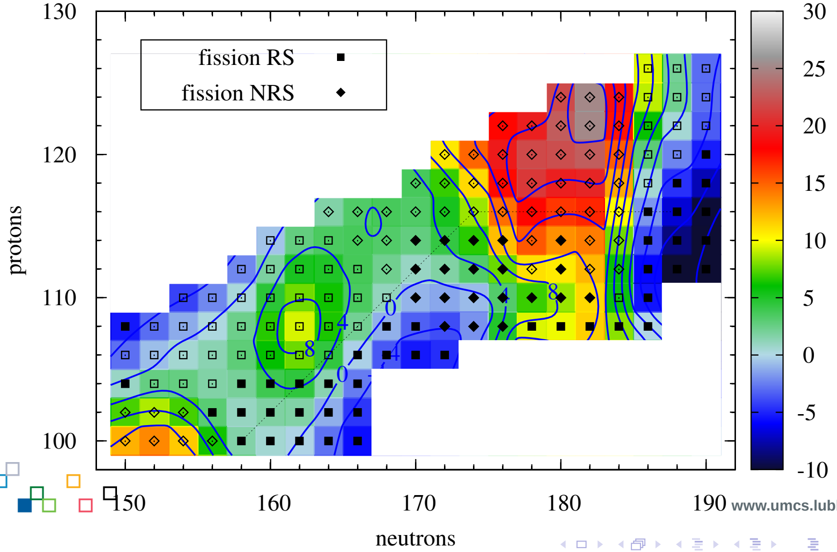

Previous approach

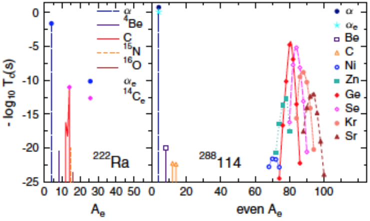

FIG. 1 (color online). Time spectra of different cluster emissions from ^{222}Ra (left panel) and from the superheavy nucleus ^{288}114 (right panel). The most probable emitted clusters from ^{222}Ra and ^{288}114 are ^{14}C and ^{80}Ge, respectively, both leading to ^{208}Pb daughter nucleus.

D. N. Poenaru, R. A. Gherghescu, and W. Greiner
Phys. Rev. Lett. 107, 062503 (2011); Phys. Rev. C 85, 034615 (2012)

ublin.pl

Cluster radioactivity - chart of nuclides

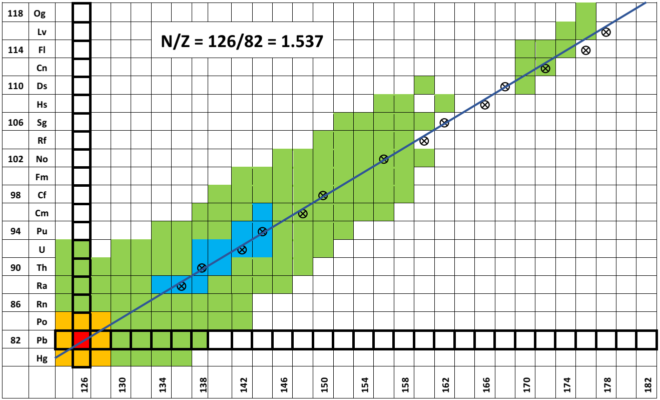

^{224}Ra

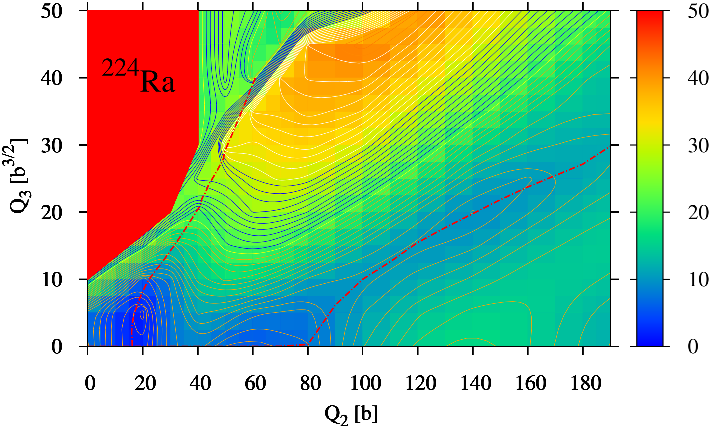

^{228}Th

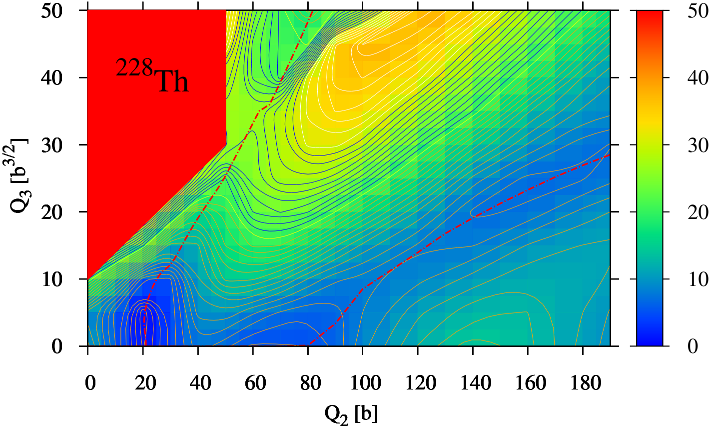

^{234}U

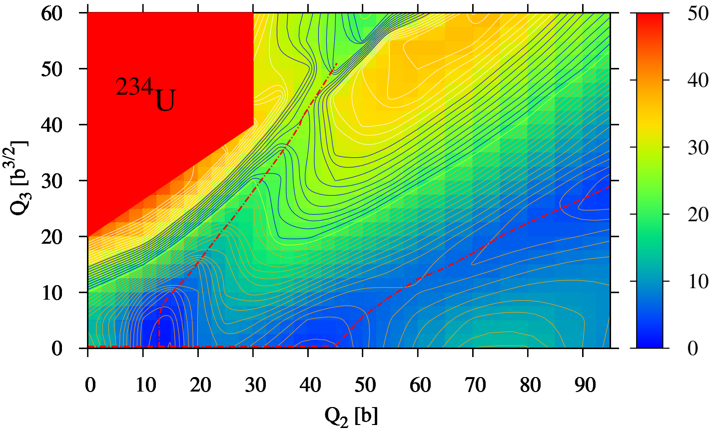

234U
60
50
40
30
20
10
0
Q3 [b3/2]
0
10
20
30
40
50
60
70
80
90
Q2 [b]
50
40
30
20
10
0

^{238}Pu

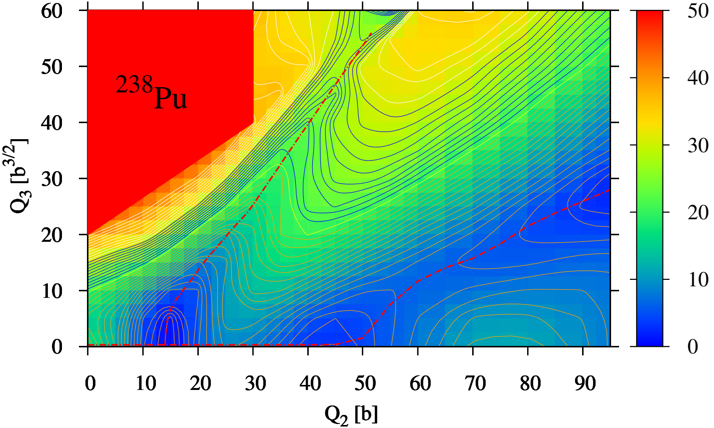

^{244}Cm

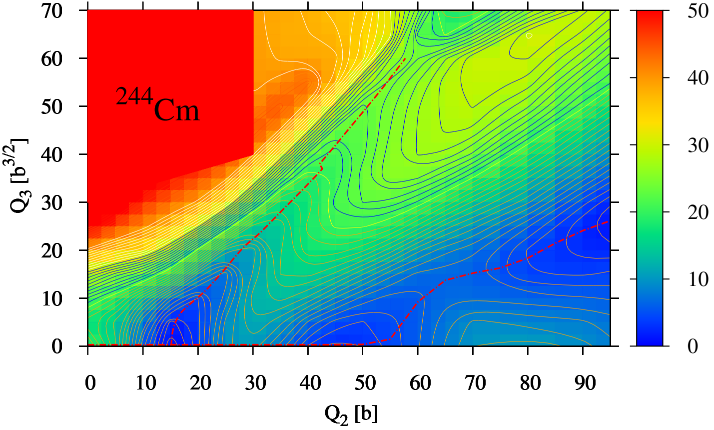

244Cm
Q3 [b3/2]
Q2 [b]
0
10
20
30
40
50
60
70
80
90
0
10
20
30
40
50
60
70
0
10
20
30
40
50

^{248}Cf

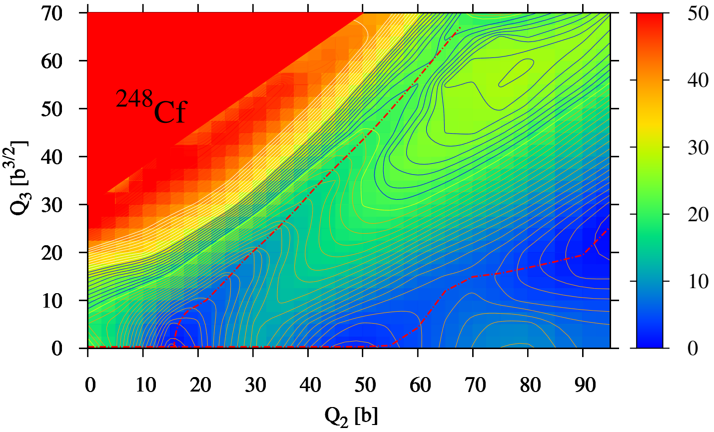
248Cf
Q3 [b3/2]
Q2 [b]
0
10
20
30
40
50
60
70
80
90
0
10
20
30
40
50
60
70
0
10
20
30
40
50

^{254}Fm

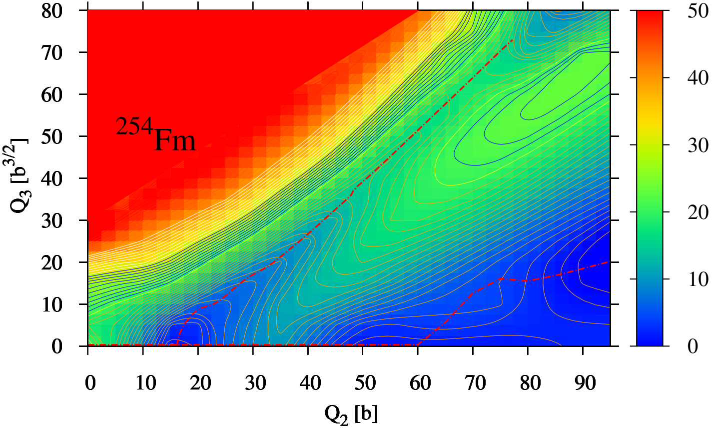

^{258}No

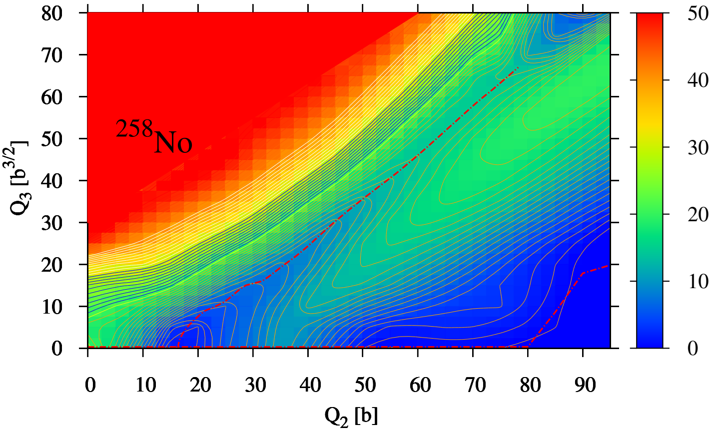

^{264}Rf

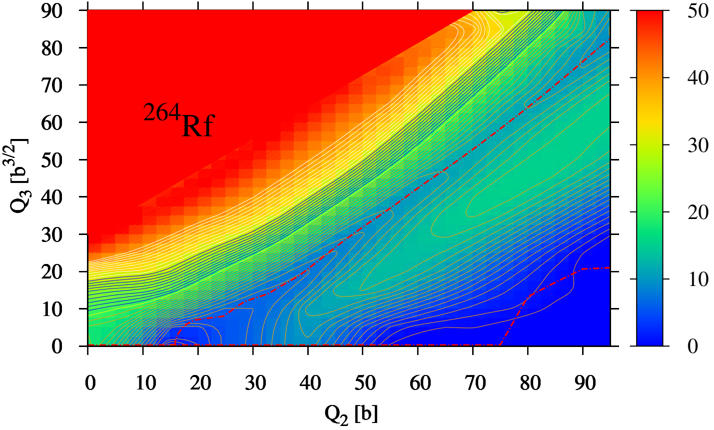

^{264}Rf
90
80
70
60
50
40
30
20
10
0
Q_3 [$b^{3/2}$]
0
10
20
30
40
50
60
70
80
90
Q_2 [b]
50
40
30
20
10
0

^{268}Sg

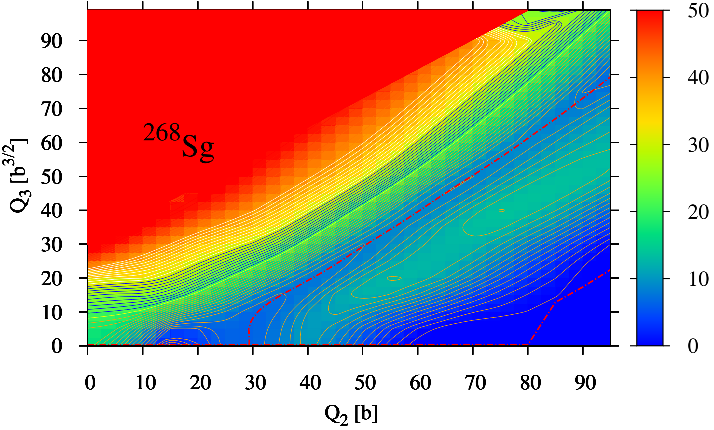

^{274}Hs

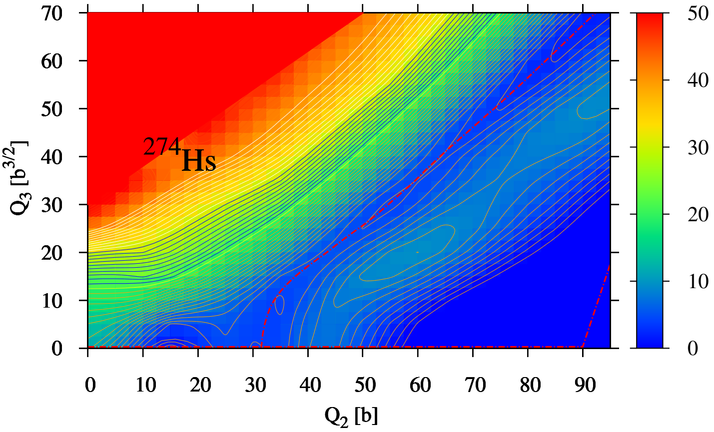

^{274}Hs
Q_3 [$b^{3/2}$]
Q_2 [b]
0
10
20
30
40
50
60
70
80
90
0
10
20
30
40
50
60
70
0
10
20
30
40
50

^{278}Ds

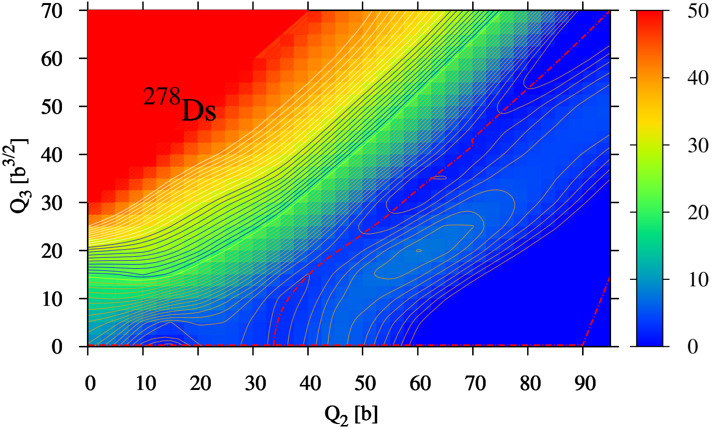
^{278}Ds
70
60
50
40
30
20
10
0
Q_3 [$b^{3/2}$]
0
10
20
30
40
50
60
70
80
90
Q_2 [b]
50
40
30
20
10
0

^{284}Cn

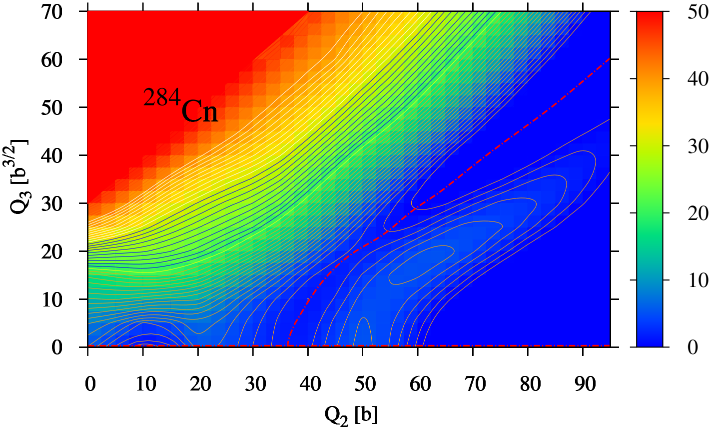

^{284}Cn
70
60
50
40
30
20
10
0
Q_3 [$b^{3/2}$]
0
10
20
30
40
50
60
70
80
90
Q_2 [b]
50
40
30
20
10
0

^{290}Fl

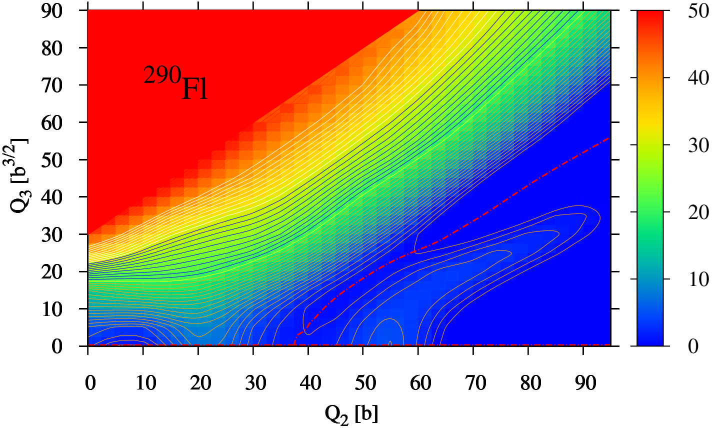

^{294}Lv

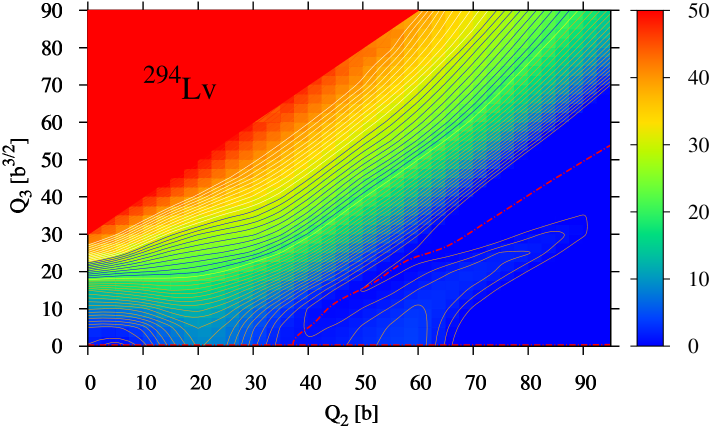

294Lv
90
80
70
60
50
40
30
20
10
0
Q3 [b3/2]
0
10
20
30
40
50
60
70
80
90
Q2 [b]
50
40
30
20
10
0

Cluster barriers

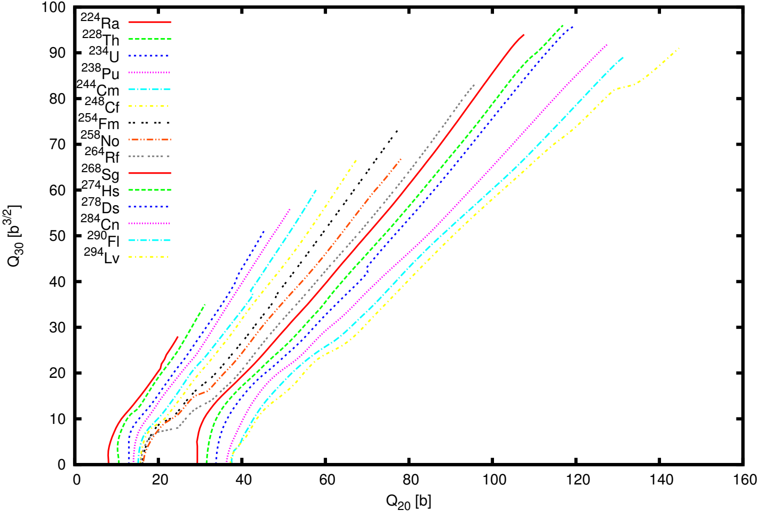

Cluster barriers

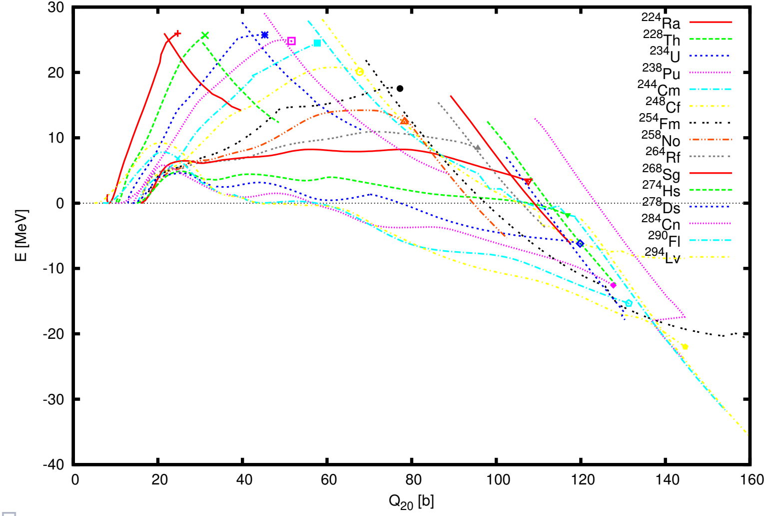

Cluster barriers

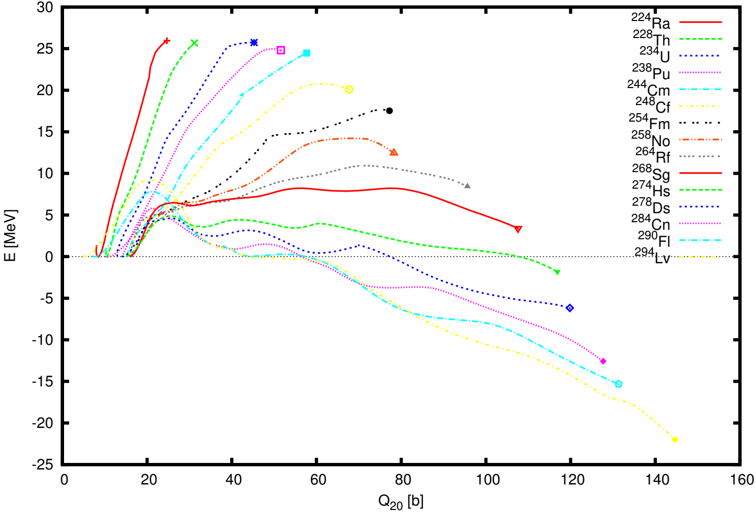

Pre-scission shapes

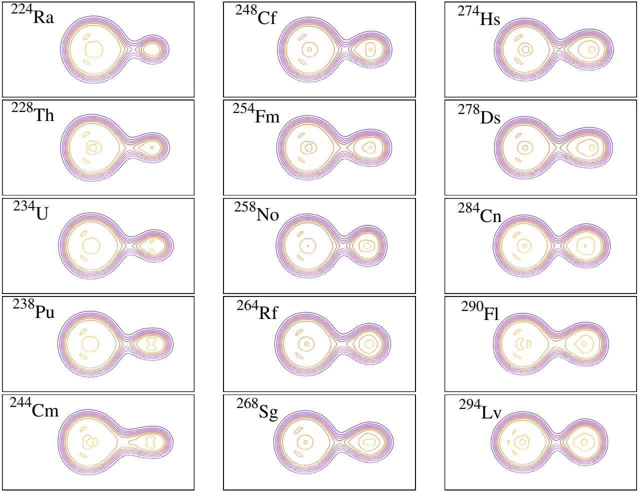

Post-scission shapes

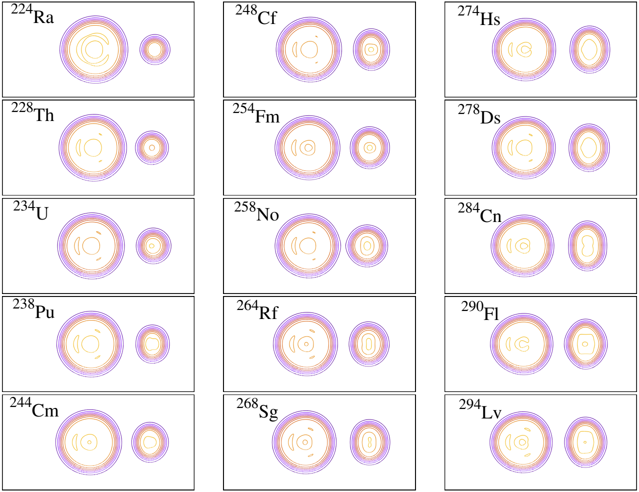

Cluster barriers

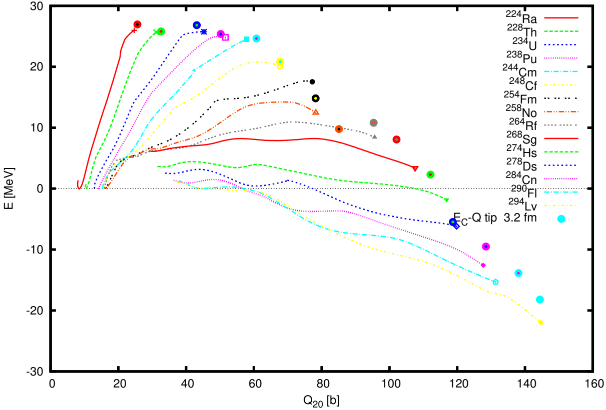

$$E = k\frac{82(Z-82)e^2}{r_{208} + r_{A-208} + d} - Q$$

Experimental evidence in ^{284}Cn:

- GSI: 9 events
  Ch. Düllmann, at al., Phys.Rev.Lett. 104, 252701 (2010)
- Dubna: 19 events
  Yu. Oganessian, Radiochim.Acta 99, 429 (2011)
- lifetimes: 30 ms - 400 ms

^{284}Cn

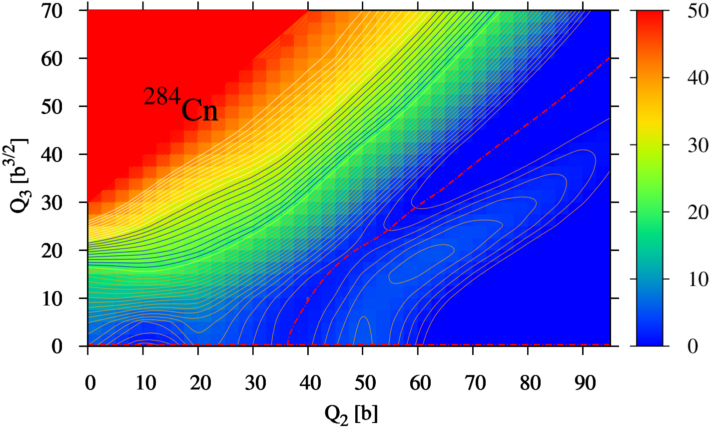

^{284}Cn
70
60
50
40
30
20
10
0
Q$_3$ [b$^{3/2}$]
0
10
20
30
40
50
60
70
80
90
Q$_2$ [b]
50
40
30
20
10
0

^{284}Cn

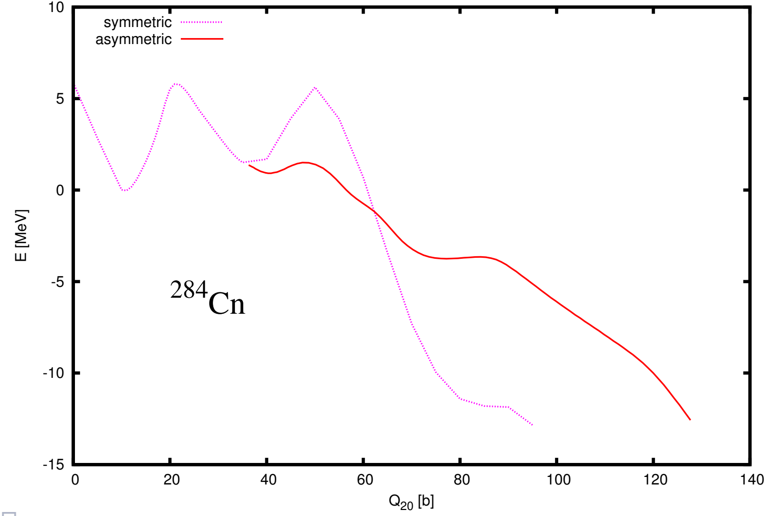
symmetric
asymmetric
E [MeV]
Q20 [b]
284Cn
10
5
0
-5
-10
-15
0
20
40
60
80
100
120
140

^{284}Cn

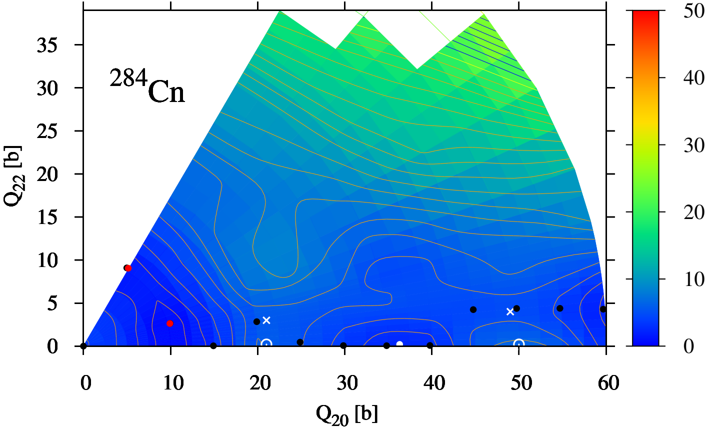
284Cn
Q22 [b]
Q20 [b]
0
5
10
15
20
25
30
35
0
10
20
30
40
50
60
0
10
20
30
40
50

Chart of SH nuclides

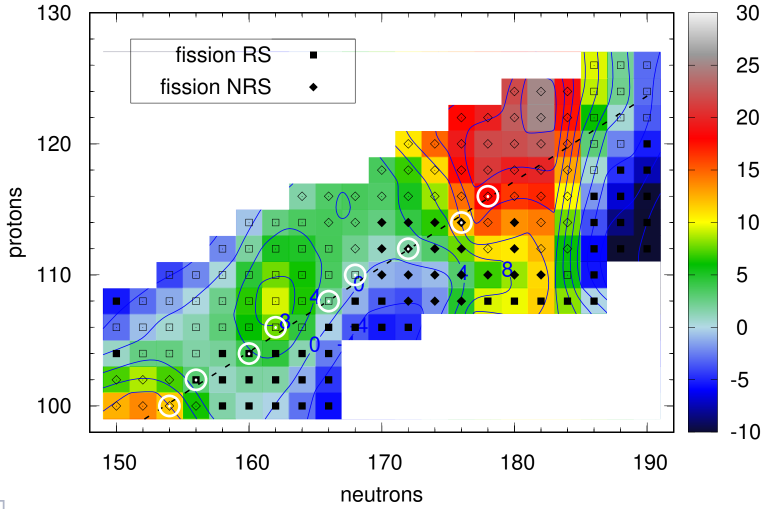

www.umcs.lublin.pl

UMCS

Actinides and superheavies

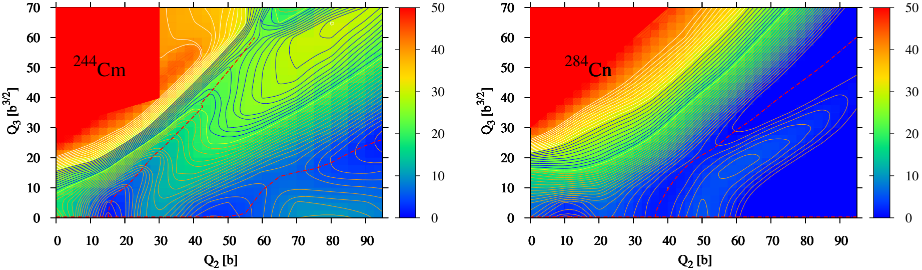

Conclusions

- Asymmetric fission in super heavy nuclei region has the same nature as cluster radioactivity in actinides
- This decay may be dominant in some super heavy nuclei
- Sharp fragment mass distribution with ^{208}Pb fragment is predicted

www.umcs.lublin.pl